Morphological determination of face-centered-cubic metallic nanoparticles by X-ray diffraction

Chi-Feng Lee, Chia-Lun Chang, Jing-Cyuan Yang, Hsiang-Yu Lai, Chun-Hua Chen *

Department of Materials Science and Engineering, National Chiao Tung University, 1001 Ta-Hsueh Road, Hsin-Chu 30010, Taiwan, ROC

ARTICLE INFO

ABSTRACT

X-ray diffraction studies of face-centered-cubic metallic nanoparticles with different morphologies are discussed based on the experimental data and the calculation of the Debye equation with the truncated and perfect strain models. At least four basic morphologies frequently observed in face-centered-cubic metallic nanoparticles, namely sphere, cube, decahedron, and icosahedron, can be clearly distinguished from their characteristic integrated intensity ratios of the first two X-ray diffraction peaks, that is, $(2 0 0)$ to $(1 1 1)$.

© 2011 Elsevier Inc. All rights reserved.

1. Introduction

Face-centered-cubic (FCC) metallic nanoparticles, for example, the most common noble elements such as Au, Ag, and Cu with various compositions, sizes, and morphologies, have been widely designed, produced, investigated, and subsequently applied in a variety of fields in the past years. A number of theoretical and experimental studies have demonstrated that the size and morphology are the most critical issues to discover the fundamentals of the distinct physical and chemical properties of nanoparticles [1–4].

Two main analytical techniques, transmission electron microscopy (TEM) and X-ray diffraction (XRD), are commonly used for nanostructural characterizations. TEM allows the size distribution, exact morphology and crystalline direction, defects, and so on of an isolated nanoparticle to be determined by direct observation of a 2D projection image. However, TEM can provide only very local information and is not suitable for densely aggregated or low-melting-point nanoparticles. In contrast, XRD can overcome these limitations and collect data from the whole specimen. By using the Debye scattering equation [5], it is possible to calculate the powder diffraction patterns of any established nanoparticle model that is related only to the variables of the chemical element and position of all atoms inside. This calculation can easily and accurately provide information on the size and morphology, especially for small mono-sized nanoparticles (≪10 nm), by qualitative and quantitative comparison of the calculated pattern profile with the experimental one, and generally shows good agreement with the TEM images [6]. In

samples containing size distributions, the particle distribution can also be extracted from quantitative comparison with calculated patterns by assuming the size distribution and particle shape. However, for larger size nanoparticles, for example, around 10 nm or above, XRD peaks with lower Miller indexes can be separated well due to the smaller full width at half maximum (FWHM). Without the great broadening and accompanying overlapping effects produced by very small nanoparticles, even when they have different morphologies, the diffraction patterns of larger nanoparticles will only show slight differences in peak profiles. For the same reason, the XRD patterns of larger nanoparticles and of bulk are rather similar and thus undistinguishable without careful and accurate numerical comparison.

In addition to the analysis problem caused by larger sizes, in frequently synthesized multiply twinned nanoparticles, for example, fivefold morphologies of icosahedrons (Ih) (20 tetrahedra) and decahedrons (Dh) (5 tetrahedra), their special morphologies are basically constructed with similar distorted tetrahedral units whose atomic arrangement is no longer FCC but rhombohedral and orthorhombic, respectively [7,8]. The overlap of the close diffraction peaks of Ih and Dh ruled by their own structural factors leads to shifted pseudo-FCC peaks with an abnormal shape and position. Consequently, supposing the larger size effects mentioned above occur in these nanoparticles, it will become much more difficult to distinguish these morphologies by using only experimental XRD raw data without any numerical analysis or precise comparison with theoretical data.

Here, we report an analytical approach to distinguish Ih, Dh, and two FCC (sphere and cube) nanoparticles with larger sizes of around 10 nm, which are frequently found in noble metallic nanoparticles prepared by physical or chemical techniques, from XRD

* Corresponding author. Fax: +886 3 5724727.
E-mail address: ChunHuaChen@mail.nctu.edu.tw (C.-H. Chen).

data. This method is based on the qualitative and quantitative comparison of experimental and theoretical XRD patterns of Ih, Dh, and two FCC nanoparticles with the assistance of TEM structural confirmation. We believe that the results as well as the analytical method are valuable for further understanding of nanostructural diffraction and are useful to distinguish at least these four metallic nanoparticles.

2. Experimental

2.1. Nanoparticle preparation

In this work, two typical cubic close-packed noble elements, Ag and Cu, were used for demonstration. Ag and Cu nanoparticles with various morphologies were prepared mainly by the polyol process to meet the requirements of high uniformity of structure and size for X-ray diffraction characterization. In this process, ethylene glycol (EG) served as both reductant and solvent, and poly(-vinyl pyrrolidone) (PVP) served as the capping reagent and stabilizer. Many studies have demonstrated that the crystal structure and morphology of the nanoparticles strongly depend on the reaction conditions, for example, the temperature, precursor concentration, and molar ratio [9,10]. For the preparation of Ag Dh nanoparticles, PVP (13.5 mmole based on the repeating unit, M_w = 10,000) was dissolved in 75 mL of AgNO$_3$ (4 mM) solution in EG. The reaction solution was stirred at 120 °C for 60 min and then allowed to cool freely to room temperature. The prepared nanoparticles were repeatedly washed by centrifugation (20 min at 10,000 rpm) with a large amount of acetone to remove most of the EG and PVP. The precipitate was then dried at room temperature for further characterization. The fabrication process of Ag cube was similar to that of Ag Dh, where the molar ratio of the repeating unit of PVP to AgNO$_3$ was 1.5 at 160 °C for 15–30 min. Cu sphere nanoparticles were synthesized, where the molar ratio of the repeating unit of PVP (M_w = 58,000) to cupric acetylacetonate (Cu(acac)$_2$) was 6.7 at 198 °C for 20 min. Cu Ih nanoparticles were obtained by the vapor condensation method as described elsewhere [11].

The TEM sample was prepared by placing a drop of the final product (suspended in ethanol) on a carbon film lying on a copper grid and dried in a fume hood. TEM images were taken on a JEOL 2100F field-emission transmission electron microscope operated at 200 kV. Nanoparticle specimens with a high morphological uniformity and narrow size distribution were first confirmed by TEM

(as illustrated in Fig. 1), and then, further XRD analysis was done. All the XRD patterns presented in this article were precisely recorded at room temperature with a Bede D1 high resolution X-ray diffractometer with monochromatized Cu Kα radiation (λ = 1.5418 Å), operated at 40 kV and 40 mA, which was used to identify the crystallite structures and sizes of the nanoparticles. In our experience, the tendencies of the morphology dependent intensity ratio revealed in this work are reproducible in many other conventional or modern X-ray diffractometers with typical powder diffraction geometry. In order to obtain a systematical result, we suggest that all specimens should be characterized by one optimized diffractometer with the same scanning parameters. In our definition, the optimized X-ray diffractometer should provide a reasonable FWHM of the strongest diffracted peak, which in the present case of FCC is the (1 1 1) peak, for the Scherrer equation for estimating an averaged particle size, which may agree with the TEM size distribution. On the specimen preparation for morphological characterization by XRD, a large amount of acetone washed nanoparticles including Ag Dh, Ag cube, and Cu sphere were repeatedly drop-cast onto Si(0 0 1) substrates to give very dense assemblies not only for obtaining high quality XRD patterns but also for evading possible morphology-induced preferential orientations. The Cu Ih nanoparticles prepared by vapor condensation were directly deposited onto MgO substrates via He flows to form a very thick black layer without any post-treatments.

2.2. Structural models

Many experimental and theoretical studies have demonstrated various Dh and Ih models including homogeneous strain [7], inhomogeneous strain with defects [12,13], and truncated models [14]. In this work, Dh and Ih nanoparticles were considered to be formed by five and 20 deformed tetrahedral units with homogeneous strain in a twin relationship, respectively. The homogeneous deformed tetrahedron unit for Dh has five edges of the smallest atomic bond length and one edge with 2% expansion relative to the other edges. In the case of Ih, three base edges have the smallest atomic bond length, and the angle between each two edges is 63.26°. This geometry generates an expansion of 5% in another three edges. Based on the homogeneous strain models, we also constructed their relative truncated models mainly based on the true morphology as observed by TEM for comparison. The Debye scattering equation used for the theoretical calculation is simply expressed as [5]:
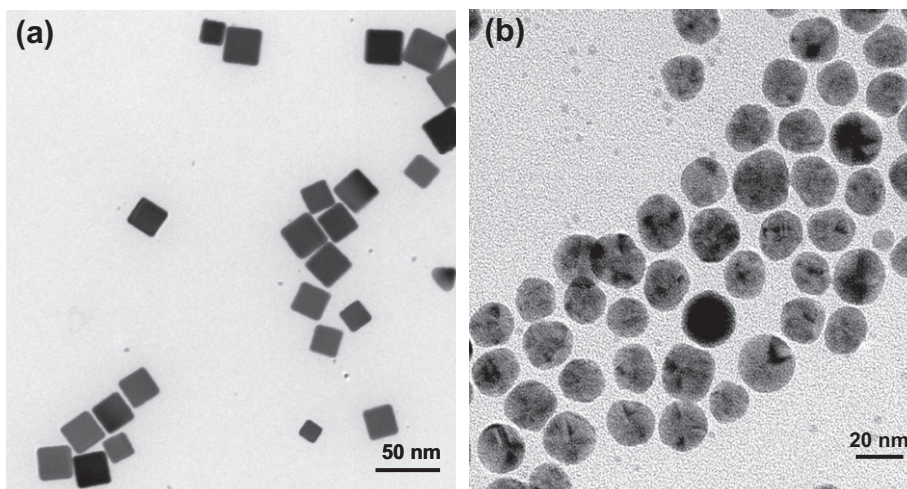

Fig. 1. The TEM images of prepared: (a) Ag cube and (b) Ag Dh nanoparticles.

$$I = \sum \sum f_m f_n \frac{\sin(qr_{mn})}{qr_{mn}}$$

where f_m and f_n are the atomic scattering factors of atoms m and n, r_{mn} is the distance between the atoms m and n, and q is expressed as $\frac{4\pi \sin\theta}{\lambda}$.

In this work, all the simulations were performed on the basis of random powders without considering preferential orientations induced by morphologies.

3. Results and discussion

Fig. 2 shows the experimental and calculated XRD patterns of the four most popular morphologies, that is, cube, Dh, Ih, and sphere. In contrast to the general whole pattern simulation for very small nanoparticles, here we focus especially on two peaks, namely (111) and (200) for cube and sphere and pseudo-(111) and pseudo-(200) for Dh and Ih, within a very local two-theta range. The
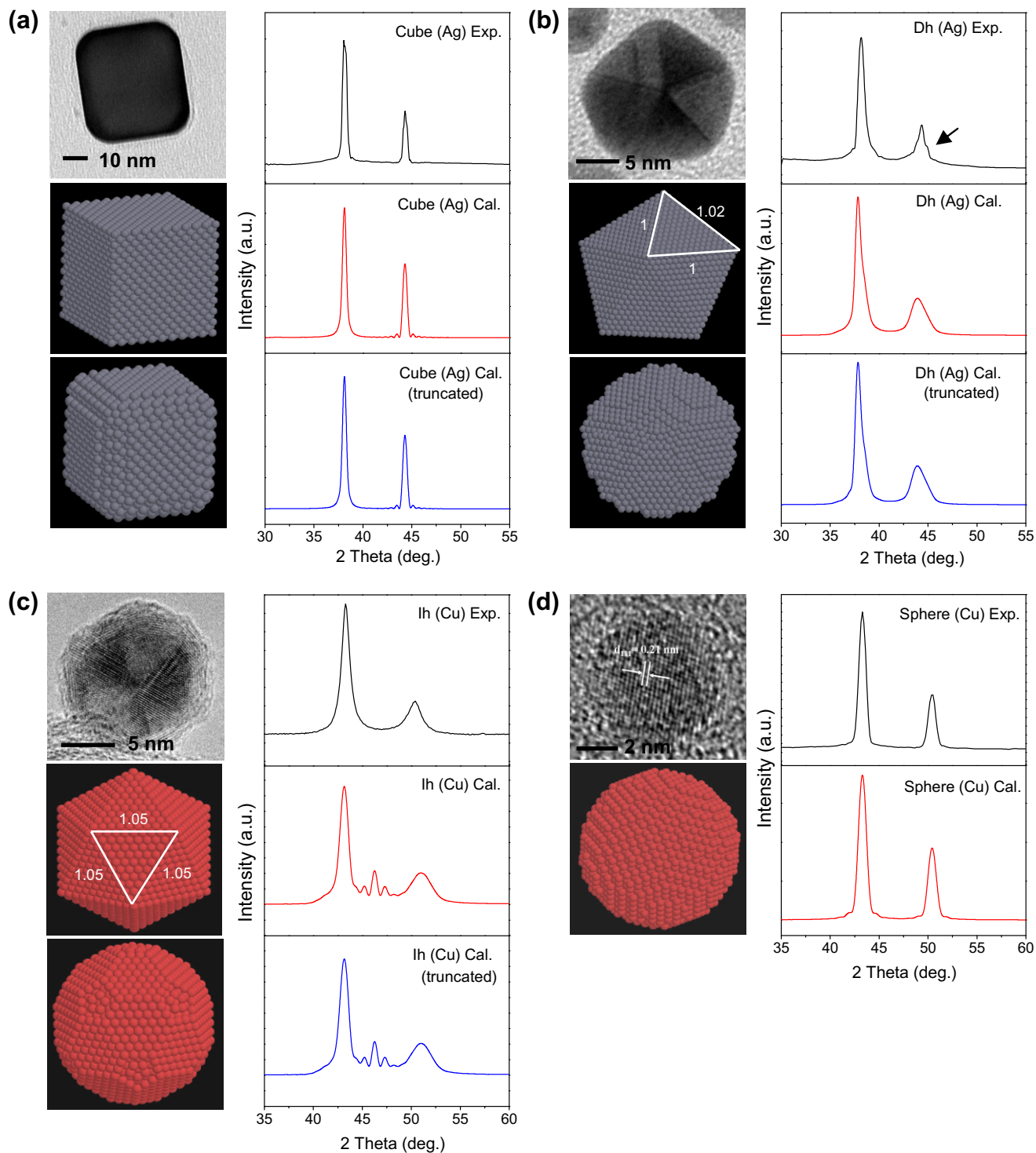

Fig. 2. The experimental XRD patterns with typical TEM images and two calculated XRD patterns with corresponding models of the four most popular morphologies, that is, (a) cube (Ag), (b) Dh (Ag), (c) Ih (Cu), and (d) sphere (Cu). In order to clearly display the details of the model structures, the model size shown here is much smaller than the one for the XRD pattern calculation.

typical TEM image of these four morphologies is illustrated with their experimental XRD data. The homogeneous strain models and the corresponding truncated ones displayed here are for demonstration purposes only. According to our previous studies, the particle size estimated from the FWHMs of the XRD peaks is in good agreement with the mean size obtained from the log-normal fitting of the TEM size distribution. Thus, the particle size used for simulation in this work was adjusted to equalize the FWHMs between the theoretical and experimental diffraction peaks. Excluding three unknown weak peaks of Ih as shown in Fig. 2c, all theoretical patterns including the homogeneous and truncated models are basically similar to the corresponding experimental ones with respect to relative peak positions, FWHMs, and even relative intensities.

In order to distinguish the differences between these morphologies, a series of integrated intensity ratios of the (2 0 0) and (1 1 1) peaks obtained by profile fitting are summarized in Table 1. It is clear that the theoretical intensity ratios for cube and sphere show very good agreement with the experimental ones, whereas larger deviations are represented for Dh as well as Ih, probably resulting from the difference between the ideal strain assumptions and the real strain conditions of the multiply twinned structures. By comparing the magnitude of the intensity ratios for these morphologies, a coincident tendency can be found, that is, sphere > cube > Dh > Ih for both theoretical and experiment results. In other words, even though the Dh and Ih models assumed here cannot provide exactly the same intensity ratios as the experimental results, the magnitude tendency is followed. Thus, these morphologies can be distinguished from the distinguishable integrated intensity ratios of XRD in practice. According to both the theoretical and the experimental data in Table 1, three clear-cut ranges of the intensity ratios can reasonably be defined: above 0.49, 0.47–0.46, and below 0.46 for sphere, cube, and Dh and Ih, respectively. Here, it is not so meaningful to identify two clear individual ranges of intensity ratio for Dh and Ih, respectively, because of the existence of greater mismatches between their theoretical and experimental data. It is reasonable to consider that this mismatch may originate from not only the simple assumption of the model but also the possible variation in size and shape of the prepared samples. However, it is worth noticing that the experimental data indeed show a distinguishable difference in intensity ratio between Dh (0.426) and Ih (0.410). These two experimental values could be the possible characteristic values for the present produced Dh and Ih nanoparticles which, respectively, contain specific strains, twin boundaries, and so on.

It is worth noticing that the second highest integrated intensity ratio of 0.47–0.46 for Ag cube is just coincident with 0.466 for Ag bulk (JCPDS: 65-2871). This coincidence originates from the fact that the cube morphology has the same crystallographic geometry as the FCC unit cell, and thus, the relative diffraction intensities of cube can be described by structural factors. This good agreement obviously evidences the reliability of the fitting results. In addition, the sphere morphology can be considered as the result of great truncation on eight corners of the cube morphology. This truncation will decrease the coherent layers of (1 1 1) and thus give a ratio of $\sim$0.49, which is higher than that of the cube.

Generally, tips, corners, and edges of nanoparticles are truncated to approach the lowest energy. Based on the TEM images in Fig. 2 and the results found in some experimental and theoretical reports [11,13–15], the truncated models, excluding sphere, are also created to allow the influence of the truncation process on intensity ratios to be understood. Fig. 3 shows the details of the three truncated models used for the present calculation. As can be seen in Table 1, the slightly truncated simulation shows no significant difference from the non-truncated simulations. Besides, this result also confirms that the intensity ratio mismatches of Dh and Ih mainly come from the complicated structures within the nanoparticles, instead of the outer fine morphologies.

To discuss the effects of internal strain conditions on the XRD patterns, we focus on the tetrahedron units of Dh and In with assumptions of various homogeneous strain conditions. For the perfect Dh as represented above, each tetrahedron unit contains 2% tensile strain along one edge. Since the original FCC structure became orthorhombic because of strain, the (1 1 1)c peak is replaced by a doublet (1 0 1)o and (0 1 1)o one and the (2 0 0)c peak by a doublet (1 1 0)o and (0 0 2)o, respectively. Thus, when a single tetrahedron unit is under this condition, a clear shoulder appears just beside the original second peak, giving an asymmetrical broadening peak as demonstrated in Fig. 4a and as found in Fig. 2b. Even though it is impossible for a normal Dh morphology to be constructed from a single tetrahedron unit with more than 2% strain, it is clear that as the strain is larger than 2%, both peaks resolve into two smaller peaks. Checking the experimental pattern of Dh in Fig. 2b, a slight shoulder can be found

Table 1
The experimental and simulated integrated intensity ratios of (2 0 0) to (1 1 1).[a]

Morphology	Experiment	Simulation	Simulation (truncated)
Sphere (Cu)	0.499	0.496	–
Cube (Ag)	0.468	0.468	0.465
Dh (Ag)	0.426	0.457	0.454
Ih (Cu)	0.410	0.448	0.450

[a] The ratios for Dh and Ih are, respectively, calculated from their pseudo-(2 0 0) to pseudo-(1 1 1).
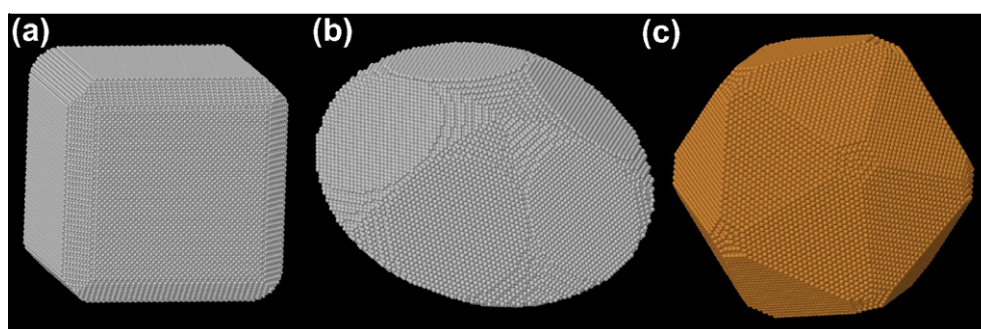

Fig. 3. The truncated models of (a) cube (265,278 Ag atoms), (b) Dh (97,558 Ag atoms), and (c) Ih (107,770 Cu atoms) used for the XRD pattern calculation.
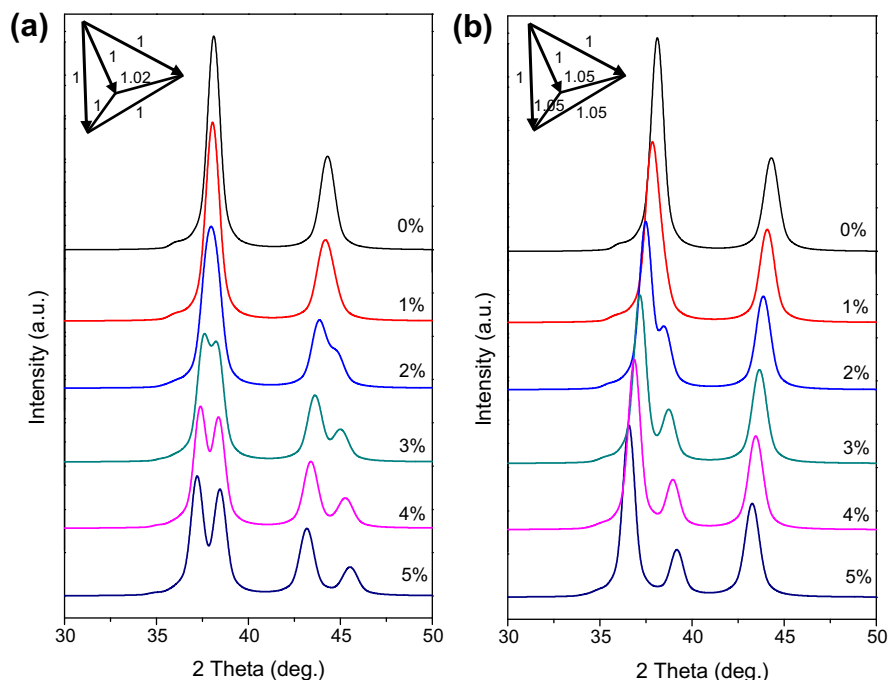
Fig. 4. The calculated XRD patterns of a single tetrahedron unit (Ag) with (a) 0~5% strain along one edge and (b) 0~5% strain along three edges.

as indexed, indicating the existence of strain of about 2% or less in the present Dh nanoparticles.

A similar process was done by assuming different strain conditions along the three edges of the tetrahedron unit of Ih as demonstrated in Fig. 4b. It is interesting that as the strain increases from 0% to 5% (the homogeneous strain model used above), one smaller unknown peak that cannot be found in the experimental data of Ih (Fig. 2c) starts to appear and grows with increasing strain. Thus, we know that the second peak of the three unknown ones in the Ih simulated pattern (Fig. 2c) might just result from the 5% homogeneous strain assumption. The other two small peaks then obviously come from the coherent scattering by atoms belonging to adjacent units. By using the Debye equation, we also evaluated every possible bond length for the production of the other two unknown peaks. However, it is still difficult to remove the specific bond lengths within the ideal strain Ih model to avoid the appearance of these peaks in the experimental pattern. These three weak peaks were less discussed before, because previous studies focused only on very small nanoparticles where the peaks completely overlapped with much stronger main peaks and were then ignored. Due to the absence of those three peaks in the experimental pattern of Ih, it is reasonable to consider that the strain conditions in the prepared Ih nanoparticles may not be as huge as in the 5% strain model. In fact, according to some TEM studies on Ih nanoparticles [12,13], defects such as extra planes or atoms can fill the gap between tetrahedron units to reduce the lattice strains.

4. Conclusions

In contrast to the general focus of the qualitative profile comparison using simulation of the whole pattern (wide two-theta range) for very small size nanoparticles (≪10 nm), in this work, we aimed to compare the intensity ratios by means of local pattern simulation for larger size nanoparticles (~10 nm). The simulated and experimental results demonstrated that at least four frequently presented morphologies of close-packing based metallic nanoparticles, that is, sphere, cube, Dh, and Ih, can be identified well from their integrated intensity ratios of the experimental XRD. The small difference in the intensity ratio between the truncated and perfect strain models indicates that the effects of truncation on the characteristic intensity ratio can be ignored for these four morphologies. The simulation with various strain conditions suggests that the lattice strains in both Dh and Ih might partially or fully relax by introducing extra atoms as observed in some TEM studies.

References

[1] B. Corain, G. Schmid, N. Toshima (Eds.), Metal Nanoclusters in Catalysis and Materials Science. The Issue of Size Control, Elsevier, Amsterdam, 2008.
[2] G. Schmid (Ed.), Nanoparticles: From Theory to Application, first ed., Wiley-VCH, 2004.
[3] C.F. Bohren, D.R. Huffman, Absorption and Scattering of Light by Small Particles, Wiley, 1998.
[4] H.Y. Lai, C.H. Chen, C.F. Lee, Plasmonics 5 (2010) 233.
[5] A. Guinier, X-ray Diffraction in Crystals, Imperfect Crystals and Amorphous Bodies, Dover, New York, 1994.
[6] N. Pinna, Prog. Colloid Polym. Sci. 130 (2005) 29.
[7] M.J. Yacamán, K. Heinenann, C.Y. Yang, H. Poppa, J. Cryst. Growth 47 (1979) 187.
[8] C.Y. Yang, M.J. Yacamán, K. Heinenann, J. Cryst. Growth 47 (1979) 283.
[9] C.X. Kan, J.J. Zhu, X.G. Zhu, J. Phys. D: Appl. Phys. 41 (2008) 155304.
[10] Y. Sun, Y. Xia, Science 298 (2002) 2176.
[11] C.H. Chen, T. Yamaguchi, K.I. Sugawara, K. Koga, J. Phys. Chem. B 109 (2005) 20669.
[12] L.D. Marks, Surf. Sci. 150 (1985) 302.
[13] J.A. Ascencio, M. Pérez, M. José-Yacamán, Surf. Sci. 447 (2000) 73.
[14] J.A. Ascencio, C. Gutiérrez-Wing, M.E. Espinosa, M. Marín, S. Tehuacanero, C. Zorrilla, M. José-Yacamán, Surf. Sci. 396 (1998) 349.
[15] P.A. Buffat, Mater. Chem. Phys. 81 (2003) 368.